Applied Physics A (2022) 128:428
https://doi.org/10.1007/s00339-022-05579-w

Applied Physics A
Materials Science & Processing

Experimental investigation on mechanical and tribological properties of the fused filament fabrication of poly-lactic acid parts with various print orientations

E. Mohan[1] · **M. Saravana Kumar**[2]

Received: 15 February 2022 / Accepted: 6 April 2022 / Published online: 22 April 2022

Abstract
Fused filament fabrication (FFF) is widely used in the domain of artificial tissue/bone engineering applications because of its capability of printing complex shapes with high efficiency. However, the mechanical properties of the 3D printed poly-lactic acid (PLA) parts are not sufficiently studied. Infill density (ID) and print orientations were the key parameters that influenced the mechanical properties of the 3D printed parts. In this research, detailed orientation studies with various ID were carried out to study the reason behind the mechanical failure of the printed materials subjected to various loads. PLA filament was used to print the 3D parts by fused depositing modelling (FDM). Three types of orientations such as horizontal (0°), inclined (45°) and vertical orientation (90°) and three types of ID percentage (60%, 80%, 100%) were considered for printing the 3D parts. The remaining input process parameters such as layer thickness, bed temperature, printing speed and infill pattern were kept constant. The 3D printed parts were carried out for mechanical evaluation such as tensile, hardness, flexural, impact and wear tests. Scanning electron microscope (SEM) was used to analyze the fractured and worn-out surfaces of the tensile, impact and wear specimens. From the mechanical testing, it was concluded that the maximum tensile strength (59 MPa), hardness (88 HRC) and flexural strength (108 MPa) was observed in the vertically oriented specimen with 100% ID and more impact strength (26 J/m) with less wear rate (9.4×10^{-3} mm^3/Nm) was evident in horizontally oriented specimens with 100% ID.

Keywords Thermoplastic · Additive manufacturing · Infill density · Tensile · Impact

1 Introduction

The additive manufacturing (AM) technology has been adopted for the manufacturing of various aerospace and biomedical applications in recent years [1]. There are various additive manufacturing processes, one of the widely used AM processes is the fused filament fabrication (FFF). Because of its easier way of printing the parts and it is cheaper. It gives low wastage of materials with higher efficiency of printing and also it can print complex shapes with the support structure [2]. Many filament materials were used in the fused deposition modelling (FDM) 3D printing such as poly-lactic acid (PLA), nylon, acrylonitrile butadiene styrene (ABS) and poly-ethylene terephthalate glycol (PETG). The thermoplastic PLA is a commonly used 3D printing material because it is a bio-degradable polymer that is suitable for tissue/bone engineering applications [3]. It also possesses good mechanical properties [4].

However, 3D printed PLA parts have several defects due to the improper print orientation and the infill density which attributes to the poor bonding between the adjacent layers. So, it was highly essential to understand the consequence of improper print orientation by evaluating the fracture morphology after the mechanical and tribological testing. The correlation between infill density and the print orientation needs to be examined to overcome the defects faced by 3D printed PLA parts.

To extend the engineering application of 3D printing technology, some studies were carried out to evaluate the

✉ M. Saravana Kumar
saravana312@gmail.com; mskumar@nitt.edu

[1] Department of Mechanical Engineering, Mount Zion College of Engineering and Technology, Pudukkottai, Tamil Nadu, India

[2] Department of Production Engineering, National Institute of Technology, Tiruchirappalli, Tamil Nadu, India

mechanical properties of the 3D printed parts [6]. Further, many surface properties of biopolymers can be improved by functionalization and surface modification of these substrates, including deposition of multi-functional coatings [5]. Liu et al. investigated the tensile performance of cellulose fiber reinforced composites which were fabricated by FDM. They have found that fiber orientation has a significant effect on fracture morphology [7]. Similarly, bronze particles were also infused into the PLA filament and evaluated its tribological properties. The presence of reinforced particles in the on-edge printed parts possesses high resistance to wear rate [8] and also enhances its biodegradability [9]. Heidari et al. found out that incorporating of continuous carbon fiber into the PLA material using the FDM shows good tensile and bending properties [10]. The high contribution of printing temperature was noted during the incorporation of nano-clay particles on the PLA filaments and the test results confirmed the enhancement of thermal stability [11]. The heat treatment was also influences the porosity [12] and the crystalline and the problem of the anisotropy of the 3D printed PLA material was overcome by optimizing the crystallinity [13]. The recycling of 3D printed materials also has a major contribution to reducing environmental problems. Research has been done to evaluate the properties of the waste PLA which was compared with the PLA with the normal grade. Even though the normal grade PLA shows good properties, the recycled PLA has a lower viscosity, higher crystallinity and less transparency [14].

The print orientation and the layer thickness have a considerable effect in enhancing the electron transfer kinetics as well as the resistivity of the conducting materials and it was proved by Abdalla et al. [15]. The tensile performance of the 3D printed PLA and the heat treated PLA materials were affected by the variation in the infill density and it was also found that the heat treated PLA materials have the maximum tensile performance with maximum infill density [16]. Similarly, varying the infill pattern such as grid, zig-zag, and concrete patterns also has a considerable effect on the tensile properties of the fabricated 3D printed PLA materials. In which zig-zag pattern depicts enhanced tensile properties [17]. But Rismalia et al. found out that the concrete pattern displays enhanced tensile properties compared with the grid and tri hexagon [18]. Gonabadi et al. proved that the increase in tensile strength and the Young's modulus was due to the increase in the infill density and also the anisotropy to the tension of the 3D printed materials were substantiated by the shear tests, shear modulus and shear rate [19]. On the comparison of 3D printed PLA and PETG material, it was verified that the 3D printed PETG materials showed improved mechanical properties but in contradiction, horizontally printed PLA materials indicate improved tribological properties when compared to 3D printed PETG materials [20]. The correlation between layer thickness and the print orientation on the surface roughness was examined by Kovan et al. [21]. They have found that the edge-oriented parts with lower layer thickness and the flat oriented 3D printed PLA parts with higher layer thickness provide enhanced bonding strength. Wickramasinghe et al. experienced that the 60% infill density with the combination of annealing effects has exhibited good wear resistance [22].

The support structure was one of the important constrain in building the 3D printed parts. Few works have been carried out to evaluate the suitable print support structure based on the orientation. Shen et al. proposed multi-objective particle swarm optimization to reduce the materials require for the support structure which can reduce the material cost and also improve the work efficiency [23]. Based on the print direction, the vibrational characteristics such as natural frequency and damping of the support structure were also examined by Singh et al. using the dynamic mechanical analyzer. From the evaluation results, it was concluded that the structure printed vertically was stiffer than the structure printed horizontally [24].

From the literature survey, it was evident that there was a lack of fracture studies based on the print orientation and the infill density. So, in this research, mechanical and tribological properties of the 3D printed PLA parts were examined based on the three types of print orientations horizontal (0°), inclined (45°) and vertical orientation (90°) and also based on the three types of infill density percentage (60%, 80% and 100%). The mechanical characterization such as tensile, harness, flexural, impact and wear test was performed. Fractured morphology (dimples, delamination, ductile and brittle fracture) and worn-out surface morphology (abrasion, plowing action, wear debris) and the bonding strength were evaluated from the results of the mechanical testing. Further, the correlation between printing direction and the loading direction was examined to evaluate the bonding strength of the printed PLA parts. This research proves that the effective print orientation and infill density enhance the mechanical and tribological properties of the printed PLA parts. These effective parameters can be adapted to the biomedical implants to enhance their mechanical strength.

2 Materials and methods

In this research, PLA (polylactic acid) material was used to print the specimen with various orientations. PLA is a bio-based biodegradable biopolymer and it is a thermoplastic polyester that was obtained from the fermentation of natural and renewable resources such as corn, cassava and sugarcane [25]. In the additive manufacturing process, the modeling of the specimen was the first step that we needed to do before starting the 3D printing [26]. The modeling of all the test specimens was done in SolidWorks 2019. The modeling

of the test specimen was based on the ASTM standards. The tensile test specimen was modeled based on the ASTM D638 Standards. The hardness specimen was modeled based on the ASTM D785 standards. The flexural strength specimen was modeled based on the ASTM D5943 standards. The Impact specimen was designed based on the ASTM D256 standards and finally, the wear specimen was modeled based on the ASTM G99 standards. Ultimaker Cura 15.04.3 software was adopted for the slicing of the modeled specimens. The designed ASTM standard specimens were converted into.STL files and then the.STL files need to be imported into the Ultimaker Cura 15.04.3 software. All the printing parameters were given as the input to the software. In this research, the adopted 3D printing parameters for building the specimens are layer height of 0.1 mm, Shell thickness of 0.8 mm, bottom/top thickness of 0.6 mm with various ID such as 60%, 80% and 100%. The printing speed of 50 mm/s, extrusion temperature of 210 °C and bed temperature of 70 °C were adopted as the speed and temperature parameters. PLA filament diameter was set as 2.85 mm with 100% flow. The nozzle size was 0.4 mm. After assigning the 3D printing process parameters, then the various orientation such as vertical (90°), inclined (45°) and horizontal (0°) orientation, need to be specified. After that, the slicing of the various orientation of specimens was examined and also ensured the support structure for the inclined oriented specimens. The G-code will be generated and then the generated G-code will be given as the input to the 3D printer [27]. So, based on the specified process parameters and G-code, the layer-by-layer printing operation was performed in the 3D printer. Drona C300 3D printer was used in this research (Fig. 1). The PLA wire filaments are inserted into the extruder setup. Initially, the heating will occur at the extruder and the printing bed until it reaches the specified bed temperature and extrusion temperature. The printing of PLA filaments begins as soon as it reaches the required extrusion and bed temperature. The layer-by-layer printing was performed based on the specified slicing. All the test specimens were printed with various IDs and orientations. The test specimen that was printed along horizontal orientation does not require a support structure and also the build specimen was parallel to the bed. Similarly, the vertically oriented specimen also does not require any support structure and also the build specimen was perpendicular to the bed [28]. But, in the inclined oriented specimen, the support structure was required. The same zig-zag infill pattern was specified for all the orientations. The printed filaments were carried out to mechanical testing. The Universal Tensile Machine was used to test the tensile strength of the 3D printed materials [6]. So, based on the load and the displacement curve obtained from the test, the tensile strength and elongation percentage were evaluated [29]. Rockwell hardness tester machine was used to analyze the hardness of the oriented samples. Five readings were taken for each specimen and the average hardness values were considered for the evaluation. Flexural testing apparatus was used to analyze the flexural strength of the printed specimen based on the 5% deflection of the printed specimen. Pendulum-type Izod impact apparatus was used for the evaluation of the impact strength of the printed specimen. The pin-on-disc tribometer was used to analyze the wear performance of the printed specimens. Various sliding distance such as 1000 m, 1250 m and 1500 m was adopted to evaluate the wear mechanism. The sliding velocity and running speed were kept constant and also the constant load of 10 N was applied to all the printed specimens. Three tests were taken for each printed specimen under each condition from which the average was considered for the evaluation. So, the wear

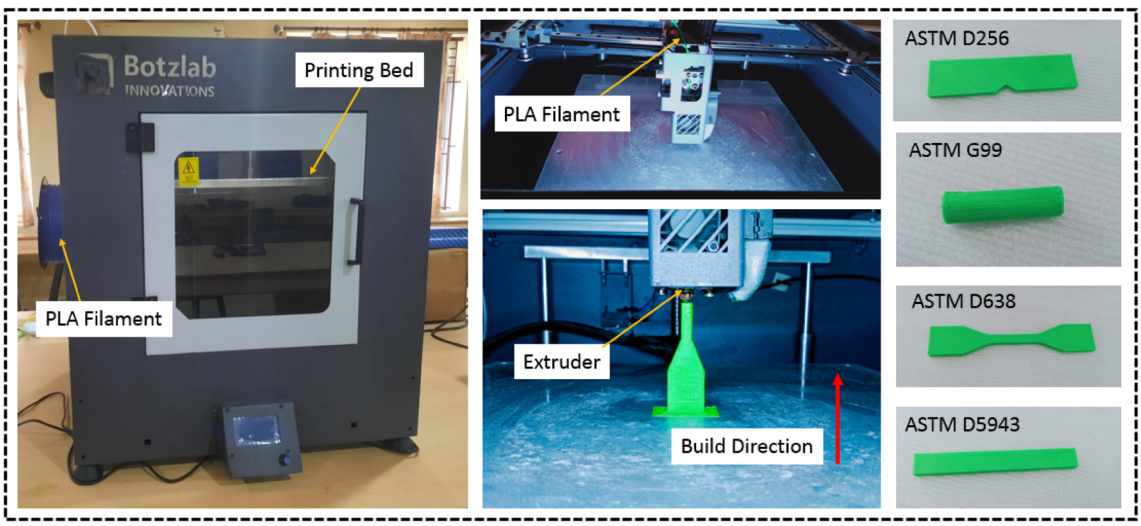

Fig.1 Pictorial representation of Drona C300 3D printer with the printed PLA specimens

rate was measured for all the printed specimens with various orientations and various IDs. Figure 2 shows the fractured specimens with various ID and print orientations.

3 Result and discussion

3.1 Tensile strength

From the results of the tensile strength (Fig. 3a), it was evident that the maximum tensile strength of 59 MPa was observed in the vertical (90°) oriented specimen with 100% ID which was perpendicular to the printing bed. The vertically oriented specimen shows 16.94% higher tensile strength when compared with the horizontal (0°) oriented specimen with 100% ID. Similarly, the maximum tensile strength of 56 MPa, 54 MPa was observed in the Vertical (90°) oriented specimen with 80% ID and 60% ID and also the lower tensile strength of 49 MPa, 45 MPa and 43 MPa was observed in the horizontal (0°) oriented specimen with 100%, 80% and 60% ID. In the case of inclined (45°) specimen, the tensile strength values range in-between the horizontal and vertical oriented specimen. Figure 4 shows the slicing of the tensile specimen printed along with the various orientation. The materials are printed layer-by-layer in 3D printing. So, we can consider the object as transverse isotropic materials [30]. Inter-layer fracture refers to the propagation of cracks between the printed layers and In-layer fracture refers to the propagation of cracks through the printed layers and the materials layer was still intact after a fracture. Mostly, in-layer fractures occur when the printing thickness of the printed specimen is small and also occur for the homogenous material. Similarly, inter-layer fractures occur at a thicker layer and in non-homogenous materials [31]. The deviation in the tensile strength was mainly due to the in-layer and inter-layer fracture. The printing direction was

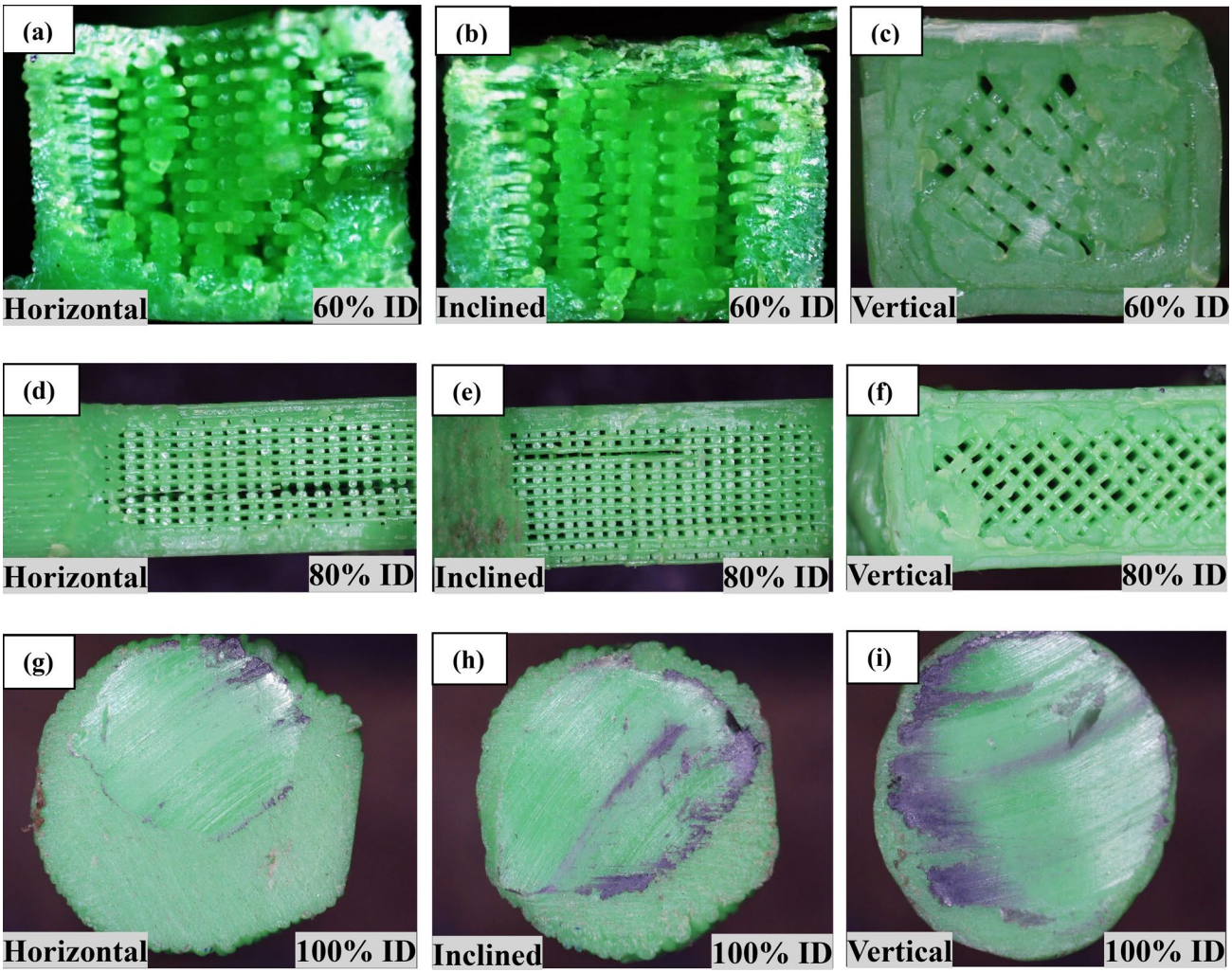

Fig. 2 Macro images of the fractured specimens **a**–**c** tensile specimens, **d**–**f** impact specimens and **g**–**i** wear specimens

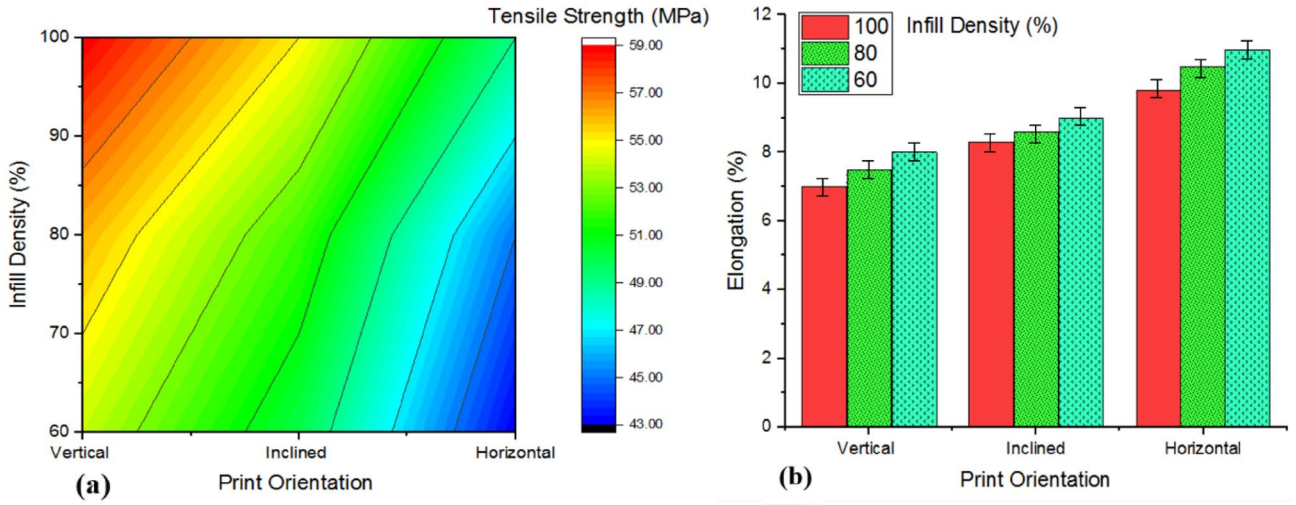

Fig. 3 Correlation between the print orientation and infill density based on the tensile strength (MPa) and elongation (%). **a** Contour plot for tensile strength (MPa). **b** Elongation% based on print orientation and infill density

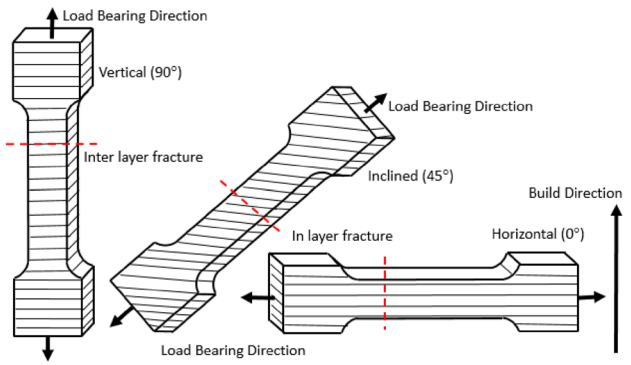

Fig. 4 Slicing diagram of tensile specimen for vertical, inclined and horizontal oriented specimens

perpendicular to the load-bearing direction in the vertically oriented specimen. So, the maximum load was required to break the bonds and also the interlayer fracture was observed in the vertically oriented specimen because the cracks propagated in between the fused layer which was the weaker bond in the vertical printed specimen. The brittle fracture was evident in the vertically oriented specimen which was shown in (Fig. 5g–i). In the case of the horizontally oriented specimen, the direction of the fusion of the materials was parallel to the load-bearing direction. So, the minimum amount of tensile force was required to break the bonds. The ductile fracture was evident in the vertically oriented specimen which was shown in (Fig. 5a–c). In-layer fracture was observed in the horizontally oriented components. Similarly, the same in-layer fracture was observed in the inclined oriented specimen because the load-bearing direction was 45° to the printing direction but the force required to break the bonds was comparatively low when compared with the vertically oriented specimen and high when compared with the horizontally oriented component. A combination of both ductile and brittle fracture was evident in the inclined oriented specimen which was shown in (Fig. 5d–f). Based on the infill density (ID), the tensile strength increases with an increase in the ID values, this was due to the creation of stronger bonds which require more tensile load to break the bonds [32]. Hence, this was the reason for the higher tensile strength in the 100% ID compared with the 80% ID and 60% ID. The high strength in 100% ID was mainly due to the closely printed layers, which increased the bonding between the printed layers [24]. The maximum elongation of 11% was observed in the horizontally oriented specimen with the 60% ID and the minimum elongation of 7% was observed in the vertically oriented specimen with the 100% ID (Fig. 3b). So, the ID plays a significant role in the elongation % of the printed specimen. It was evident that, if the ID increases, then the elongation increases which considerably affects the tensile property of the printed specimen.

3.2 Hardness strength

From the hardness test results, the maximum hardness value of 88 HRC was observed in the vertically oriented specimen with 100% ID which was 18.18% higher than the vertically oriented specimen with 60% ID. Figure 6a shows the contour plot for hardness values (HRC) and Fig. 6b shows the bar chart representing the hardness values (HRC) based on print orientation and infill density. It was observed that the maximum harness value in the vertically oriented samples was due to the resistance to the indentation effect. The printing direction was perpendicular to the direction of the

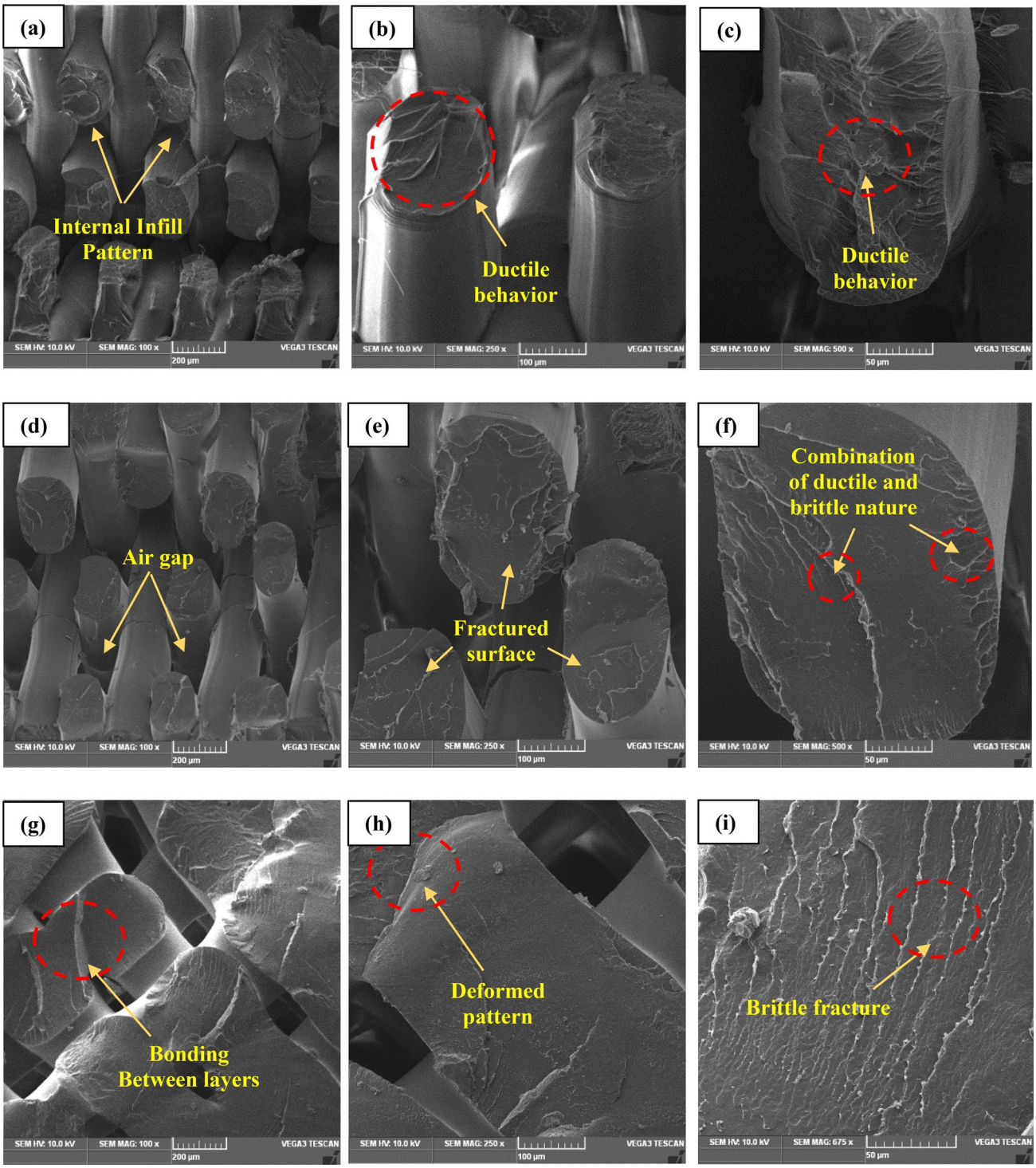

Fig. 5 SEM image of the fractured morphology of the tensile specimen at **a–c** horizontal, **d–f** inclined and **g–i** vertical orientation

indentation effect. The indentation was restricted by the fusion of materials along the surface which has a strong bond compared to the other orientation. So the maximum hardness values were obtained on the building surface i.e. top surface [33]. Similarly, the minimum hardness value of 65 HRC was observed in the horizontally oriented sample with 60% ID which was 20.73% lower than the horizontally oriented specimen with 100% ID. In the case of the horizontally oriented component, the lower hardness was due to the weaker bonds between the layers. Figure 7 shows the

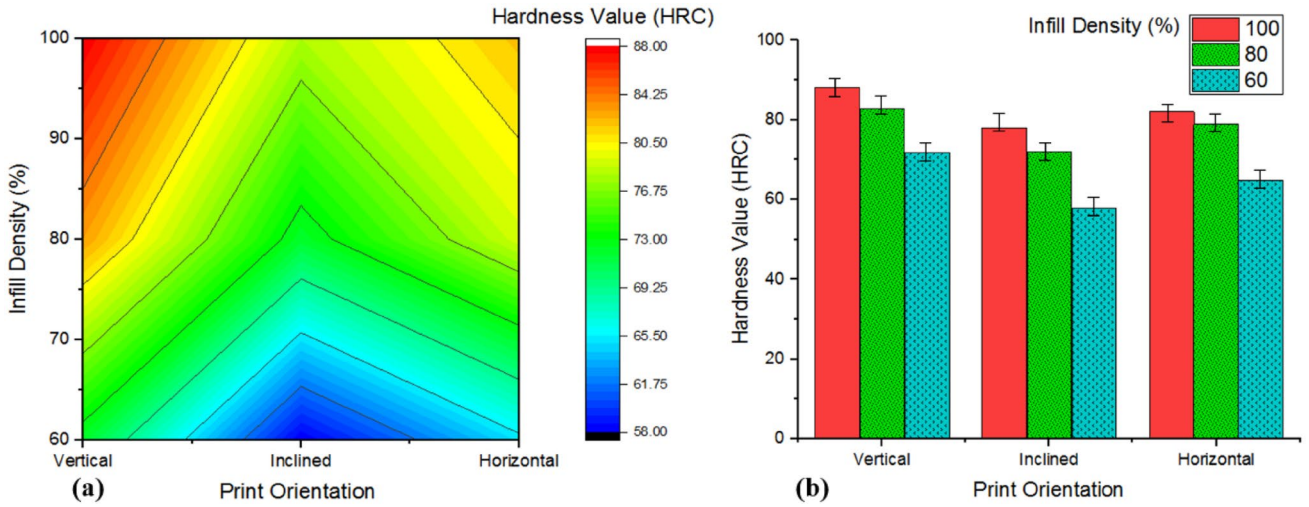

Fig. 6 Correlation between the print orientation and infill density based on the rockwell hardness (HRC). **a** Contour plot for hardness values (HRC). **b** Bar chart representing the hardness values (HRC) based on print orientation and infill density

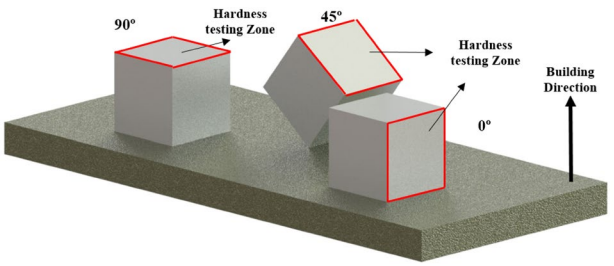

Fig.7 Hardness specimens with vertical, inclined and horizontal orientation

orientation of the hardness specimen. Tiny lines of grooves were observed in-between the printed layers which affects the hardness values along the side surface of the build specimen and also the lower hardness on the side surface was due to the indentation load which was parallel to the direction of the build specimen [34]. In the case of the inclined specimen, the hardness values were lower when compared with both the vertical and the horizontal oriented specimens. A maximum hardness value of 78 HRC was observed in the inclined oriented samples with 100% ID which was 25.64% higher than the inclined oriented sample with 60% ID. Similarly, the inclined specimen exhibits a similar effect but 4.87% and 11.36% lower than the horizontally and vertically oriented specimen. More fluctuation was observed in the inclined oriented specimens. High hardness values were obtained in the fused region and lower hardness values were obtained in between the layers. So, based on the average, lower hardness value was evident on the inclined surface. It was evident that the maximum infill density makes the specimen heavier which leads to solid print and resists the indentation effect. So, the 100% ID exhibits better hardness.

3.3 Flexural strength

From the flexural strength results, it was evident that the maximum flexural strength of 108 MPa was observed in the horizontally oriented specimen with 100% ID which was 18.5% higher than the specimen printed along with the horizontal orientation with 60% ID. Figure 8a shows the contour plot for flexural strength (MPa) and Fig. 8b shows the bar chart representing flexural strength values (MPa) based on print orientation and infill density. The maximum flexural strength was required for the 5% deflection of the horizontally oriented specimen, this was because the load-bearing direction was perpendicular to the building direction. So, the maximum load was required to deflect the horizontally oriented specimen. During the applied load, the top surface of the horizontally oriented specimen exhibits compression stress and the bottom surface, it exhibits tensile stress. The build direction of the 3D printed specimen helps to restrict both the stress which creates the maximum stiffness [27]. Figure 9 shows the slicing diagram of the tensile specimen printed along with the various orientation. The minimum flexural strength of 82 MPa was observed in the vertically oriented component with 60% ID which was 10.8% lower than the vertically oriented specimen with 100% ID. The minimum flexural strength was required for the 5% deflection of the vertically oriented specimen, this was due to the fusion of particles along the building direction and also the load-bearing direction was parallel to the direction of the building of the specimen [35]. So the low resistance to

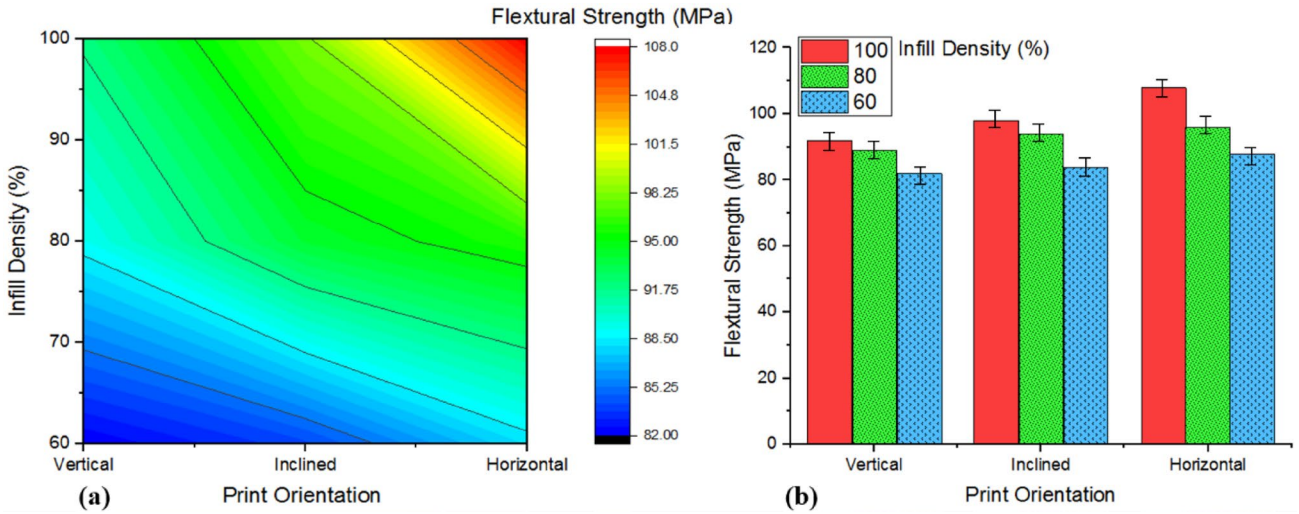

Fig. 8 Correlation between the print orientation and infill density based on the flexural strength (MPa). **a** Contour plot for flexural strength (MPa). **b** Bar chart representing the flexural strength values (MPa) based on print orientation and infill density

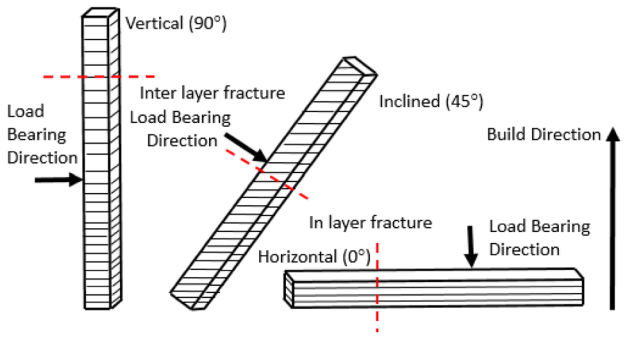

Fig. 9 Slicing diagram of flexural specimens for vertical, inclined and horizontal oriented specimens

deformation was provided by the vertically oriented specimen. In the case of an inclined oriented specimen, the maximum flexural strength of 98 MPa was observed in the 100% ID which was 14.8% higher than the specimen printed with 60% ID. The flexural strength values vary in-between the horizontal and vertical oriented specimen for the inclined specimen. This was because the building direction was 45° inclined to the direction of the load applied. It was observed that the higher thickness was evident in the inclined oriented specimen than in the other oriented sample and also the stepwise structure was observed on the surface. In terms of ID%, maximum flexural strength was observed in the 100% ID which was due to the compact printing without any air gap and that leads to more stiffness and finally, attributes to the increase in the flexural strength.

3.4 Impact strength

From the results of the impact strength (Fig. 10), it was evident that the maximum impact strength of 26 J/m was obtained on the horizontally oriented sample with 100% ID which was 38.46% higher than the horizontally oriented specimen with 60% ID. Figure 10a shows the contour plot for impact strength (J/m) and Fig. 10b shows the bar chart representing impact strength values (J/m) based on print orientation and infill density. Figure 11 shows the slicing of the impact specimen along the various orientations. The maximum impact strength observed in the horizontally oriented samples was because the direction of the impact load was perpendicular to the direction of the fusion of the PLA materials. So, the high resistance was offered by the specimen's building direction, which restricts the dislocation movements. In-layer fracture was observed in the horizontally oriented parts. The propagation of the cracks was restricted by each layer of the printed specimen (Fig. 12g–i). So, this was the reason behind the maximum impact strength. The minimum impact strength of 12 J/m was observed on the vertically oriented specimen with 60% ID which was 33.33% lower than the vertically oriented sample with 100% ID. In the case of the vertically oriented specimen, the direction of the impact load was parallel to the building direction [33]. So, only less impact load was required for the propagation of the cracks along with the fused layers [36]. Inter-layer fracture was observed in the vertically oriented parts. The cracks propagate between the fused layers were due to the poor bonding of the materials which results in lower impact strength (Fig. 12a–c). Nominal impact strength of 22 J/m

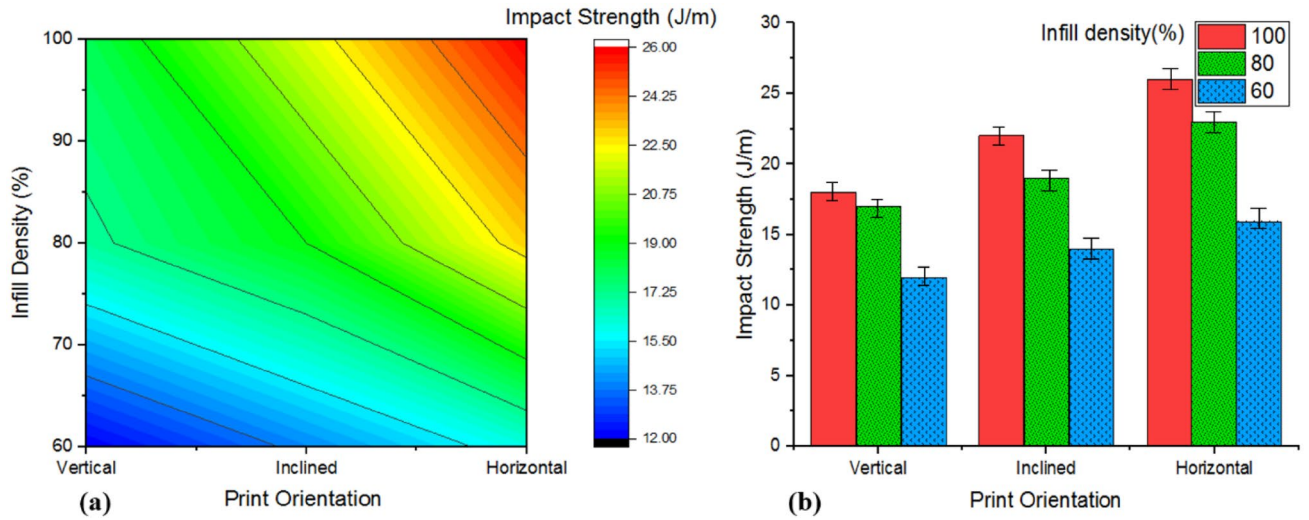

Fig. 10 Correlation between the print orientation and infill density based on the impact strength (J/m). **a** Contour plot for impact strength (J/m). **b** Bar chart representing the impact strength (J/m) based on print orientation and infill density

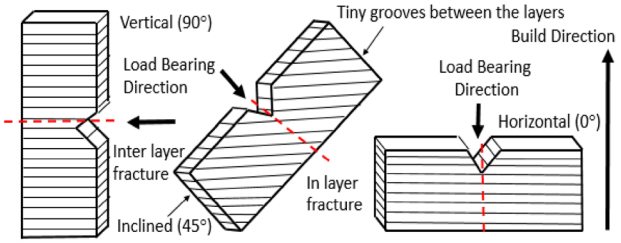

Fig. 11 Slicing diagram of impact specimens for vertical, inclined and horizontal orientations

was observed on the inclined oriented specimen with 100% ID which was 36.36% higher than the inclined oriented specimen with 60% ID. In the inclined oriented specimens, the inter-layer fracture was observed (Fig. 12d–f). The direction of the impact load was 45° to the specimen's build direction, which was the reason for the nominal impact strength. So, the required load for the impact failure was lower when compared to the horizontally oriented specimen and higher when compared to the vertically oriented specimen. It was also observed that the infill density plays a significant effect on the impact strength of the 3D printed specimens. It was evident that the increase in the ID value increases the impact strength of the specimens which was confirmed by the constant improvement in the impact strength in all the orientations.

3.5 Wear strength

The wear test was performed on the specimens with various orientations. The progressive damage was observed due to the sliding contact between the two parts. The material loss was evaluated and the wear rate was analyzed. The material loss was due to the rubbing of parts concerning a certain relative motion. The 10 N load was applied to the wear specimen which was kept constant for all the orientations. Various sliding distance was adopted such as 1000 m, 1250 m, and 1500 m. From Fig. 13b–d, it was observed that the wear rate of the printed specimen increases with the increase in the sliding distance. This was mainly due to the increase in the contact time between the specimen and the counterpart surface. From the wear rate analysis (Fig. 13a), it was observed that the specimen printed along the horizontal orientation had a less wear rate of 9.4×10^{-3} mm^3/Nm when compared with the other oriented specimens. Figure 14 shows the splicing diagram of the wear specimen along with the various orientation. In the horizontally oriented specimen, the sliding slide was perpendicular to the building direction. So, the rear rate was restricted by the multiple layers along the sliding surface (Fig. 15g–i). More abrasion was evident in the horizontally oriented specimen which was due to the perpendicular building direction which refers to the proper bonding between the printed layers [37]. More wear rate was observed in the specimen with 60% ID and less wear rate was observed in the specimen with 100% ID. So, the infill density has a considerable effect in decreasing the wear rate of the printed specimen. A more wear rate of 14.9×10^{-3} mm^3/Nm was observed on the vertically oriented specimen with 60% ID which was 6.04% higher than the vertically oriented specimen with 100% ID. This proves that the wear rate increases with the decrease in the infill density (Fig. 15a–c). More wear debris was evident in the vertically oriented specimen which led to the plowing of the materials [37]. So the wear debris will act as the second body abrasion which consecutively leads to a more wear

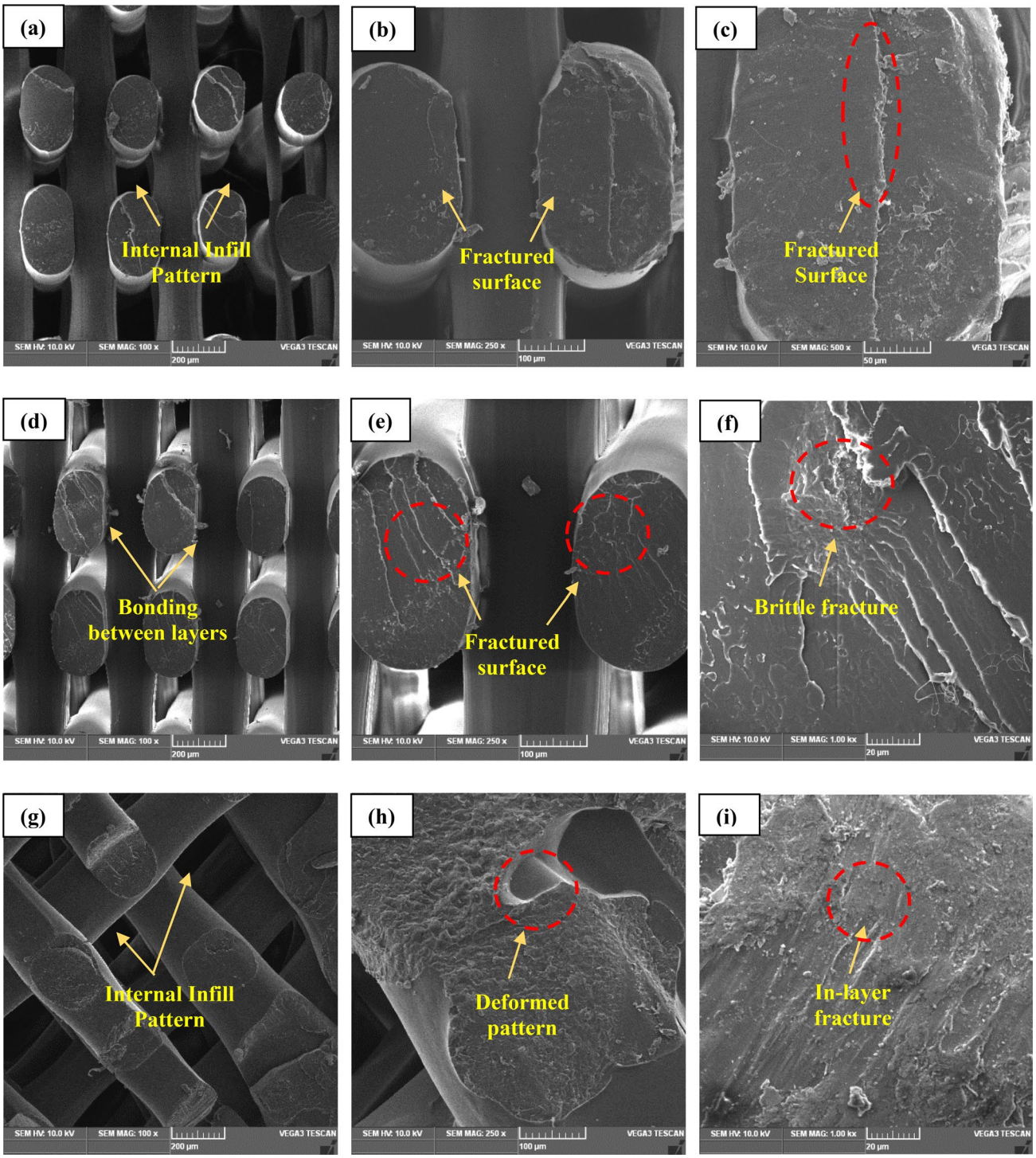

Fig. 12 SEM image of the fractured surface of the impact specimen at **a–c** vertical, **d–f** inclined and **g–i** horizontal orientation

rate. The sliding side was parallel to the building direction in the vertically oriented specimen. So, the maximum wear rate was observed in this orientation. For the inclined oriented specimen, the wear rate was higher when compared to the horizontally oriented specimen and lower when compared to the vertically oriented samples. In the inclined oriented specimen, the sliding side was 45° to the building direction. Even though the multiple layers restricted the wear rate (Fig. 15g–i), wear debris formed during the sliding will form as the second body abrasion which increases the wear rate of the inclined specimen.

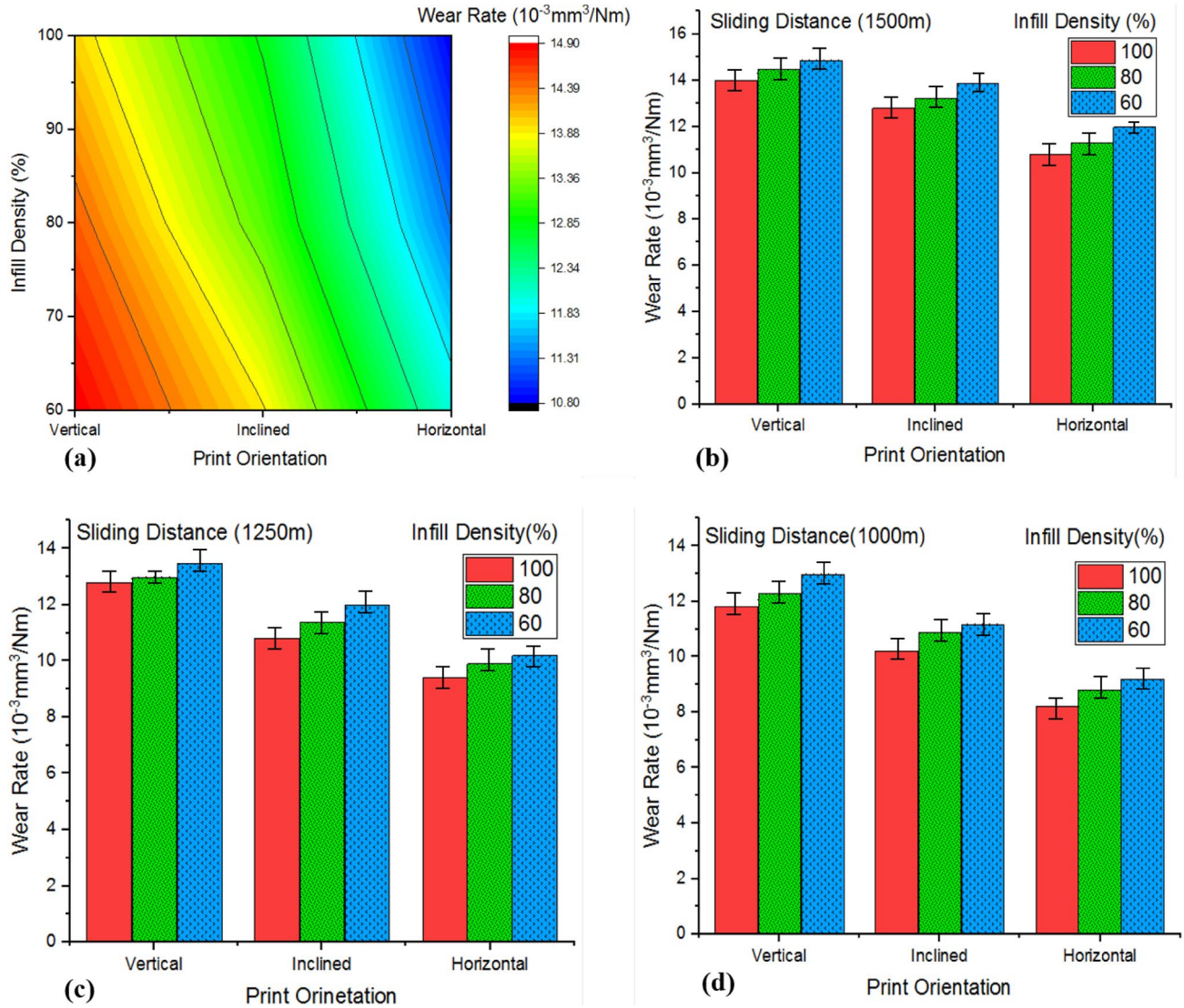

Fig. 13 Correlation between the print orientation and infill density based on the wear strength. **a** Contour plot for wear rate, **b** 1500 m sliding distance, **b** 1250 m sliding distance, **b** 1000 m sliding distance

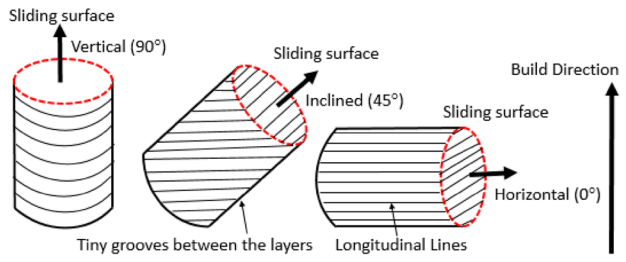

Fig. 14 Slicing diagram for the wear specimens for vertical, inclined and horizontal orientations

4 Conclusion

The 3D printed PLA parts were tested for their tensile, hardness, flexural, impact and wear strength based on the horizontal, inclined and vertical orientation with various ID. Based on the results, the following conclusions were made.

- The vertically oriented specimens with 100% ID exhibit 16.94% higher tensile strength and that represents the strong bonding between the layers which resists the

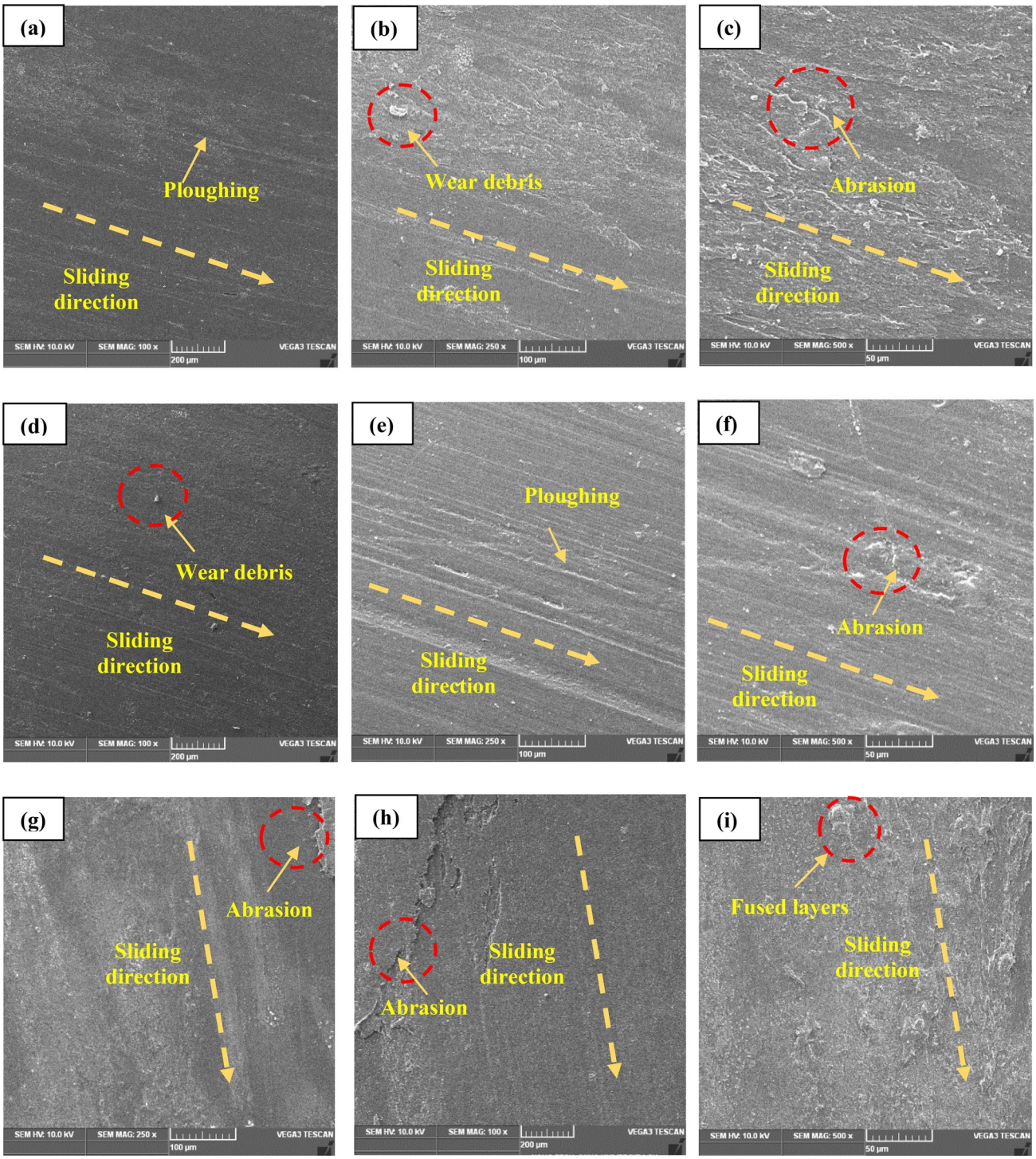

Fig. 15 SEM image of the worn-out surface of the wear specimen at **a–c** vertical, **d–f** inclined and **g–i** horizontal orientation

deformation moment along the vertical direction. Moreover, the brittle fracture was observed in the vertically oriented parts and the ductile fracture was observed in the horizontally oriented parts.

- The indentation effect was highly restricted by the vertically oriented PLA parts with 100% ID. But, horizontally oriented parts with 60% ID shows 20.73% reduced resistance towards penetration effect due to the maximum porosity.
- The maximum flexural strength of 108 MPa was observed in the horizontally oriented specimen with 100% ID. This was due to the strong bonding force by each binding layer

that resists the bending force exerted to the printed parts. But in contradiction, vertically oriented components with 60% ID exhibits poor resistance towards the bending moment.

- The maximum impact strength of 26 J/m was obtained on the horizontally oriented sample with 100% ID and that proves the ability of the PLA material to resist the propagation cracks on the horizontally oriented parts. But vertically oriented parts influence the crack propagations and that attributes to the minimum impact strength of 12 J/m.
- The specimen printed along the horizontal orientation exhibits high resistance towards plowing action and that leads to the lower wear rate of 9.4×10^{-3} mm^3/Nm. Similarly, more wear rate was observed in the specimen having 60% ID and less wear rate was observed in the specimen having 100% ID.

Author contributions All authors contributed to the study conception and design. Material preparation, data collection and analysis were performed by EM and MSK. All authors read and approved the final manuscript.

Funding The authors did not receive support from any organization for the submitted work.

Availability of data and materials The raw/processed data required to reproduce these findings cannot be shared at this time as the data also forms part of an ongoing study.

Declarations

Conflict of interest The authors have no conflicts of interest to declare that are relevant to the content of this article.

References

1. L. Li, Q. Sun, C. Bellehumeur, P. Gu, Composite modeling and analysis for fabrication of FDM prototypes with locally controlled properties. J. Manuf. Process. **4**(2), 129–141 (2002). https://doi.org/10.1016/S1526-6125(02)70139-4
2. S. Rashia Begum, M. Saravana Kumar, M. Vasumathi et al., Revealing the compressive and flow properties of novel bone scaffold structure manufactured by selective laser sintering technique. Proc. Inst. Mech. Eng. Part H J. Eng. Med. **1**, 2–56 (2022). https://doi.org/10.1177/09544119211070412
3. G. Cicala, D. Giordano, C. Tosto, G. Fillippone et al., Polylactide (PLA) filaments a biobased solution for additive manufacturing: correlating rheology and thermomechanical properties with printing quality. Materials (Basel). (2018). https://doi.org/10.3390/ma11071191
4. S. Rashia Begum, M. Saravana Kumar, C.I. Pruncu et al., Optimization and fabrication of customized scaffold using additive manufacturing to match the property of human bone. J. Mater. Eng. Perform. **30**(7), 4848–4859 (2021). https://doi.org/10.1007/s11665-020-05449-7
5. A. Kyzioł, K. Kyzioł, Surface functionalization with biopolymers via plasma-assisted surface grafting and plasma-induced graft polymerization—materials for biomedical applications. In: Biopolymer grafting, pp. 115–151. (2018).
6. M. Saravana Kumar, E. Mohan, S. Robinson et al., Comparative study on morphological, physical and mechanical characteristics of L-PBF based AlSi10Mg parts with conventional stir casted Al-10%SiC composites. SILICON (2021). https://doi.org/10.1007/s12633-021-01065-9
7. H. Liu, H. He, X. Peng et al., Three-dimensional printing of poly(lactic acid) bio-based composites with sugarcane bagasse fiber: effect of printing orientation on tensile performance. Polym. Adv. Technol. **30**(4), 910–922 (2019). https://doi.org/10.1002/pat.4524
8. M.M. Hanon, Y. Alshammas, L. Zsidai, Effect of print orientation and bronze existence on tribological and mechanical properties of 3D-printed bronze/PLA composite. Int. J. Adv. Manuf. Technol. **108**(1–2), 553–570 (2020). https://doi.org/10.1007/s00170-020-05391-x
9. G.S. Sivagnanamani, S.R. Begum, R. Siva et al., Experimental investigation on influence of waste egg shell particles on polylactic acid matrix for additive manufacturing application. J. Mater. Eng. Perform. (2021). https://doi.org/10.1007/s11665-021-06464-y
10. M. Heidari-Rarani, M. Rafiee-Afarani, A.M. Zahedi, Mechanical characterization of FDM 3D printing of continuous carbon fiber reinforced PLA composites. Compos. Part B Eng. **175**(October 2018), 107147 (2019). https://doi.org/10.1016/j.compositesb.2019.107147
11. B. Coppola, N. Cappetti, L. Di Maio et al., 3D printing of PLA/clay nanocomposites: influence of printing temperature on printed samples properties. Materials (Basel) **11**(10), 1–17 (2018). https://doi.org/10.3390/ma11101947
12. X.F. Shen et al., Effect of heat treatments on the microstructure and mechanical properties of Al–Mg–Sc–Zr alloy fabricated by selective laser melting. Opt. Laser Technol. (2021). https://doi.org/10.1016/j.optlastec.2021.107312
13. Y. Liao et al., Effect of porosity and crystallinity on 3D printed PLA properties. Polymers (Basel) **11**(9), 1–14 (2019). https://doi.org/10.3390/polym11091487
14. F.R. Beltrán et al., Technical evaluation of mechanical recycling of PLA 3D printing wastes. Polymers (Basel). (2021). https://doi.org/10.3390/polym13081247
15. A. Abdalla, H.H. Hamzah, O. Keattch et al., Augmentation of conductive pathways in carbon black/PLA 3D-printed electrodes achieved through varying printing parameters. Electrochim. Acta **354**, 136618 (2020). https://doi.org/10.1016/j.electacta.2020.136618
16. M.M. Hanon, R. Marczis, L. Zsidai, Influence of the 3D printing process settings on tensile strength of PLA and HT-PLA. Period. Polytech. Mech. Eng. **65**(1), 38–46 (2021). https://doi.org/10.3311/PPme.13683
17. C.K. Yeoh, C.S. Cheah, R. Pushpanathan et al., Effect of infill pattern on mechanical properties of 3D printed PLA and cPLA. IOP Conf. Ser. Mater. Sci. Eng. (2020). https://doi.org/10.1088/1757-899X/957/1/012064
18. M. Rismalia, S.C. Hidajat, I.G.R. Permana et al., Infill pattern and density effects on the tensile properties of 3D printed PLA material. J. Phys. Conf. Ser. **1402**(4), 2–8 (2019). https://doi.org/10.1088/1742-6596/1402/4/044041
19. H. Gonabadi, A. Yadav, S.J. Bull, The effect of processing parameters on the mechanical characteristics of PLA produced by a 3D FFF printer. Int. J. Adv. Manuf. Technol. **111**(3–4), 695–709 (2020). https://doi.org/10.1007/s00170-020-06138-4

20. M.M. Hanon, R. Marczis, L. Zsidai, Impact of 3D-printing structure on the tribological properties of polymers. Ind. Lubr. Tribol. **72**(6), 811–818 (2020). https://doi.org/10.1108/ILT-05-2019-0189
21. V. Kovan, G. Altan, E.S. Topal, Effect of layer thickness and print orientation on strength of 3D printed and adhesively bonded single lap joints. J. Mech. Sci. Technol. **31**(5), 2197–2201 (2017). https://doi.org/10.1007/s12206-017-0415-7
22. S. Wickramasinghe, T. Do, P. Tran, FDM-based 3D printing of polymer and associated composite: a review on mechanical properties, defects and treatments. Polymers (Basel) **12**(7), 1–42 (2020). https://doi.org/10.3390/polym12071529
23. H. Shen, X. Ye, G. Xu et al., 3D printing build orientation optimization for flexible support platform. Rapid Prototyp. J. **26**(1), 59–72 (2020). https://doi.org/10.1108/RPJ-09-2018-0252
24. Singh, K.V., Khan, F., Veta, J, et al., Influence of printing orientation on the dynamic characteristics and vibration behavior of 3D printed structures. In: International Design Engineering Technical Conferences and Computers and Information in Engineering Conference, American Society of Mechanical Engineers, vol. 58110, p. V001T02A032 (2017).
25. J. Fernandes, A.M. Deus, L. Reis et al., Study of the influence of 3D printing parameters on the mechanical properties of PLA. Proc. Int. Conf. Prog. Addit. Manuf. **2018**, 547–552 (2018). https://doi.org/10.25341/D4988C
26. I. Tirado-Garcia et al., Conductive 3D printed PLA composites: on the interplay of mechanical, electrical and thermal behaviours. Compos. Struct. **265**, 113744 (2021). https://doi.org/10.1016/j.compstruct.2021.113744
27. J. Wang, H. Xie, Z. Weng et al., A novel approach to improve mechanical properties of parts fabricated by fused deposition modeling. Mater. Des. **105**, 152–159 (2016). https://doi.org/10.1016/j.matdes.2016.05.078
28. M.S. Kumar, H.R. Javidrad, R. Shanmugam et al., Impact of print orientation on morphological and mechanical properties of L-PBF based $AlSi_7Mg$ parts for aerospace applications. SILICON (2021). https://doi.org/10.1007/s12633-021-01474-w
29. M. Saravana Kumar, M. Vasumathi, S. Rashia Begum et al., Medium-term absorption kinetics and thermal stability analysis of hybrid fiber metal laminate and experimental investigations on its physical and tensile properties. Polym. Compos. **42**(8), 4155–4165 (2021). https://doi.org/10.1002/pc.26203
30. B.A. Aloyaydi, S. Sivasankaran, H.R. Ammar, Influence of infill density on microstructure and flexural behavior of 3D printed PLA thermoplastic parts processed by fusion deposition modeling. AIMS Mater. Sci. **6**(6), 1033–1048 (2019). https://doi.org/10.3934/MATERSCI.2019.6.1033
31. J.S. Shim, J.E. Kim, S.H. Jeong et al., Printing accuracy, mechanical properties, surface characteristics, and microbial adhesion of 3D-printed resins with various printing orientations. J. Prosthet. Dent. **124**(4), 468–475 (2020). https://doi.org/10.1016/j.prosdent.2019.05.034
32. S. Ranganathan, K. Kumar, S. Gopal et al., The effect of print orientation and infill density for 3D printing on mechanical and tribological properties. SAE Tech. Pa.p (2020). https://doi.org/10.4271/2020-28-0411
33. Y. Song, Y. Li, W. Song et al., Measurements of the mechanical response of unidirectional 3D-printed PLA. Mater. Des. **123**, 154–164 (2017). https://doi.org/10.1016/j.matdes.(2017).03.051
34. S. Kumar, R. Singh, T.P. Singh et al., On mechanical characterization of 3-D printed PLA-PVC-wood dust-Fe_3O_4 composite. J. Thermoplast. Compos. Mater. **35**(1), 36–53 (2022). https://doi.org/10.1177/0892705719879195
35. J.A. Afonso, J.L. Alves, G. Caldas et al., Influence of 3D printing process parameters on the mechanical properties and mass of PLA parts and predictive models. Rapid Prototyp. J. **27**(3), 487–495 (2021). https://doi.org/10.1108/RPJ-03-2020-0043
36. M. Dawoud, I. Taha, S.J. Ebeid, Effect of processing parameters and graphite content on the tribological behaviour of 3D printed acrylonitrile butadiene styrene. Materwiss. Werksttech. **46**(12), 1185–1195 (2015). https://doi.org/10.1002/mawe.201500450
37. P.K. Bajpai, I. Singh, J. Madaan, Tribological behavior of natural fiber reinforced PLA composites. Wear **297**(1–2), 829–840 (2013). https://doi.org/10.1016/j.wear.2012.10.019